Wind-Induced Sediment Dynamics Impact on Turbidity for Watrerworks in Taihu Basin Based on Numerical Simulation

Xinyu Yao (yaoxinyu@zju.edu.cn)
Zhejiang University
Xiaowei Liu
Zhejiang University
Yongchao Zhou
Zhejiang University
Liang Zhang
Huzhou Water Group
Zhixu Zhou
Huzhou MeteorologicalBureau
Yiping Zhang
Zhejiang University https://orcid.org/0000-0001-8537-8181

Research Article

Keywords: suspended sediment concentration, waterworks, turbidity, numerical simulation, wind condition, lag effect

Posted Date: January 28th, 2022

DOI: https://doi.org/10.21203/rs.3.rs-1241223/v1

Abstract

Lake Taihu is an important drinking water source for cities of Yangtze River Delta region, while the dramatically fluctuate of turbidity caused serve problems for local waterworks' management. Since the sediment behavior induced by wind disturbance was believed to be the main factor for the matter, the effect of wind fields on hydrodynamic and sediment distribution of Lake Taihu and the turbidity of the raw water were conducted based on wind driven numerical model. The results indicate that wind direction was more influential for the structure of flow and wave fields while wind speed contributed more to the field intensity, and the suspended sediment of the water intake area was primarily consisted of migrated particles from other erosion regions. The high consistence between the simulated suspended sediment concentration and the turbidity with a lag effect of 7-hour made it possible for turbidity prediction when combined with weather forecast technique. The model achieved operation adjusting in advance, thus improve the management efficiency of the waterworks.

Highlights

1. The raw water turbidity of Lake Taihu was primarily determined by wind field
2. A wave-current coupled model driven by winds was developed for turbidity prediction
3. The one-year series of modeling SSC and turbidity shared high similarity with a pattern distance of 0.55
4. The 7-hour lag between simulated and real data enables waterworks to adjust operation promptly

1 Introduction

Turbidity is a crucial index to evaluate the quality of drinking water for waterworks, which can provide shelter for pathogenic micro-organisms. However, the violent fluctuations of it cause problems for dosage adjustment and further operational performance, especially for waterworks with large shallow lakes as supplies. Owning to open water-sediment interface and small depth, shallow lakes are more susceptible to wind field, which made the sediment behavior induced by wind disturbance become the main attribution of turbidity variation (Kessarkar et al. 2009; Wu et al. 2013). When the wind blows over a large shallow lake, wind energy is quickly absorbed by the water-air interface and transferred to the bottom layer through breaking waves and turbulence, once the bottom shear stress is sufficiently large, the sediment layer could be loosened (Bohling 2009) and particles would be stimulated into overlying water body resulting in a large sediment flux (Tang et al. 2019). To study the effect of wind-induced hydrodynamics on sediment action and achieve the prediction of suspended sediment concentration (SSC), numerous researches have been taken at some well known shallow water bodies, such as Lake Balaton in Hungary (Luettich et al. 1990), Lake Biwa in Japan (Kumagai 1988), Lake Okeechobee in the United States (Jin and Ji 2001), and so on. Luettich et al.(1990) presented a simple model for the depth-averaged suspended sediment concentration based on surface wave height. The model neglected vertical variations in SSC, horizontal transport, and temporal variations in the particle size distribution and

seemed acceptable in SSC forecasting. Chao et al. (2008) applied a cohesive sediment transport model to Deep Hollow Lake, a small oxbow lake in Mississippi. The model obtain a generally good agreement by considering the bottom shear stresses induced by currents and waves, and the processes of resuspension, deposition, settling. Zhang et al. (2015) explored a scheme for assimilating remotely sensed suspended sediment into a two-dimensional sediment transport model of Poyang Lake in China, and got reasonable spatial patterns of suspended sediment.

As a typical shallow lake in China, Lake Taihu is the third largest freshwater lake with a water surface area of 2388.1 km^2 and a mean depth of 1.9 m. It is located in the lower Yangtze delta (Fig. 1) and become an important drinking water source for 38 cities (population coverage of approximately 60 million) around. For the large water-soil contact and the flat underwater terrain, the lake is frequently disturbed by wind and has experienced large-scale resuspension of sediment. The correspondingly acute fluctuation of turbidity left little time to waterworks to adjust the operating parameter. A large number of studies have been conducted in Lake Taihu to investigate the impacts of wind-induced currents and waves on sediment behavior, and attempted to forecast the SSC or even turbidity through field observations, laboratory experiments, numerical modelings and machine learning models. The bottom shear stress generated by wind-induced waves has been certified to be the main dynamic force for sediment behavior in shallow water bodies (Wu et al. 2013; Luo et al. 2004), while the shear stress caused by lake flows can be ignored for the negligible effect (Qin et al. 2005; Stone 2011). The wave shear stress contributed more than 70% to local particles resuspension in shallow lakes and this value even reached 95% in Lake Taihu (Sheng and Lick 1979; Li et al. 2016). Most field studies and experiments were devoted to studying the relationship between wind fields and sediment concentration, further defining the incipient motion of sediment action in the lake. Qiu et al. (2013) simulated the resuspension of sediments from Zhushan Bay under different wind forcing by laboratory experiments, the work established exponential functions between SSC and flow velocity and proposed an incipient velocity of about 0.21 m/s. Wu et al. (2013) developed a simple turbidity model with a sound physical basis based on in situ high-frequency observations of short-term and strong wind-induced sediment suspension, the model considered the vertical migration of particles and simulated turbidity of the data collection site successfully. Jalil, et al., (2019) found a second-order polynomial fitting correlation between wave, current, and total shear stress with SSC at Meiliang Bay, and got a critical wind speed range of 4~6 m/s through high-frequency measured data. Tang et al. (2020) took wind fetch into account and proposed that both wind speed and wind fetch could effectively lead to sediment resuspension. Tthe incipient motion of the action is a wind speed of 4 m/s with long fetch and considerable sediment enter the overlying water when wind speed reaches to 5~6m/s. However, sediment sampled from the collection site is difficult to maintain the original characteristics and conditions in the laboratory are all simplified, thus causing great deviations from the practical condition. Furthermore, the observed data is always from a single site, which is inadequate to reflect the spatial distribution of sediment in the lake (Li et al. 2016). Numerical simulation was then commonly used to imitate the hydrodynamics and sediment field of the entire lake Models covering the entire water surface take more actual factors into consideration, such as boundary conditions and sediment transportation, which are all crucial for sediment process. Qiu et al.

(2013) simulated the sediment distribution in the FVCOM model. The model was driven by the varying wind field and validated with the satellite retrieval. Li (2016) studied the flow and wave distribution of the lake under prevailing wind conditions and manifested that the closed circulations formed during the hydrodynamic process may increase the SSC and contaminant concentration here. Since turbidity is a complex index affected by physical, chemical, and biological factors, describing it quantitatively as well as accurately predicting is difficult. Techniques from the field of Machine Learning, such as Artificial Neural Network (ANN) (Kennedy et al. 2015), Genetic Algorithm (GA) (Burchard-Levine et al. 2014; Aani et al. 2019), Support Vector Machine (SVM) (Wang et al. 2009) have been shown to be suitable predictors for non-linear data.

Although extensive efforts have been made to studying the influencing mechanism of wind force on sediment distribution and making a precise forecast, study about turbidity prediction was relatively infrequent for numerous influence factors and the sophisticated interaction among them. What's more, the field study highlighted the temporal distribution of a single observation site while ignoring the impact of the spatial distribution (i.e., the effect of transportation). Rather, model results from numerical simulation were always used to analyze the spatial response of sediment under wind action but seldom related to a certain observation site. And the machine learning model was always lack of interpretability. Therefore, simulation of flow, wave, shear stress and sediment fields driven by wind fields from MIKE 21/3 software, as well as the recorded high-frequency turbidity data of raw water in Taihu waterworks were used in the current study to: (1) observe the impact of wind speed and direction upon hydrodynamic and sediment distribution of the lake; (2) estimate the SSC and understand the sediment source of the water intake area under different wind conditions; (3) investigate the response intensity of simulated SSC on turbidity and explore the potentiality of turbidity prediction based on numerical simulation.

2 Methods And Models

2.1 Study area

Lake Taihu (30°56'~31°33' N and 119°53'~120°36' E) is an important drinking water source for many local cities, the city of Huzhou, Zhejiang Province is one of the beneficiaries. The Taihu waterworks located here pump raw water from east Taihu Lake through two 7.6-kilometer-long diversion pipes, and the water-supply covers more than 400 square kilometers and over one million residents. The water intake (Fig. 1) is close to the bank with an average water depth of about 1 m, the shallowness makes the wind-induced waves and currents easier to cause intense hydrodynamic disturbance in the water body, and further turbidity increase at the study site. The dramatic fluctuation of the influent turbidity has resulted in serve problems for waterworks' management. Therefore, the current study is devoted to investigating how wind fields affect the turbidity of raw water and exploring the potentiality to turbidity prediction based on field simulation. The meteorological station closest to the water intake, Pulou (30°56'00" N, 120°17'57" E) station, was selected as the observation site (Fig. 1).

2.2 Data collection

The wind field data (wind speed, wind direction) of Pulou Station were provided by Huzhou Meteorological Observatory of Zhejiang Province with a interval of 1 hour. And the historical turbidity data were acquired from Taihu Waterworks. Hourly data of the raw water pumped from the water intake was automatic recorded by a Hach online turbidity. In addition, the cyanobacteria concentration of the water intake area with a interval of 4 hour was also collected from Huzhou Environmental Monitoring Center to observe the contribution of alga to the turbidity. All real time data sets used in this study were in a period of year 2020 (from January 1, 2020 to December 31, 2020).

2.3 Modeling

2.3.1 Governing Equations

MIKE 3 has been widely used in areas such as oceans, coastal regions, estuaries, and lakes, which uses incompressible Reynolds-averaged Navier-Stokes equations and adopts Buossinesq approximation and hydrostatic assumption. This study used MIKE 3 to set up numerical simulation models to analysis the waves, flows and sediment pattern of Lake Taihu under diversified wind conditions. In consideration of the dominant force and type of sediment in the lake, the following modules were selected: the HD (Hydrodynamic) and the Mud Transport (MT) module from MIKE 3 software package, the SW (Spectral Waves) module from MIKE 21/3 software package. The HD module and SW module achieved bidirectional coupling by sharing hydrodynamic information obtained in HD module and the wave factors calculated in SW module (Kuang et al. 2016). The MT module is linked to the 2D wave module (SW) and 3D hydrodynamic model of the current (HD), and uses modeled data for calculation of sedimentation processes, simultaneously.

The SW model bases on unstructured meshes, and the fully spectral formulation was adopted in this study. The wave action balance equation is described as follows(Komen et al. 1994).

$$N(\sigma, \theta) = E(\sigma, \theta) / \sigma \quad (1)$$

where N is the action density, E is the energy density, θ is the wave component direction (°), and σ is the relative angular frequency (r/s), the spectrum is limited to the range between a minimum (σ_{min}) and maximum (σ_{max}) value.

The evolution of the wave spectrum in position (x, y) and time (t) (Hasselmann et al. 1973) is:

$$\frac{\partial}{\partial t}N + \frac{\partial}{\partial x}C_x N + \frac{\partial}{\partial y}C_y N + \frac{\partial}{\partial \sigma}C_\sigma N + \frac{\partial}{\partial \theta}C_\theta N = \frac{S_{SW}}{\sigma} \quad (2)$$

$$(C_x, C_y) = \frac{dx}{t}, C_\sigma = \frac{d\sigma}{t}, C_\theta = \frac{d\theta}{t} \quad (3)$$

where $\vec{x}$= (x, y) is the Cartesian co-ordinates; C_x, C_y, C_θ, and C_θ are the propagation velocities in x, y, σ and θ space, respectively; S_{SW} is the source term for the energy balance equation. The radiation stresses,

S_{xx}, S_{xy}, S_{yx} and S_{yy} (m^3/s^2), significant wave height, H_s (m) and zero-crossng wave period T_z (s) used in HD model are derived from SW model:

$$H_s = \sqrt{E} \quad (4)$$

$$T_z = \sqrt{E / \left(\int_0^{2\pi}\int_0^{\sigma_{max}} E(\sigma, \theta)\sigma^2 d\sigma d\theta + \frac{\sigma_{max}^3}{2}\left[\int_0^{2\pi} E(\sigma_{max}, \theta) d\theta\right]\right)} \quad (5)$$

$$S_{xx} = \frac{1}{2} g \left(\int_0^{2\pi}\int_0^{\infty} \left(cos^2\left(\frac{3}{2}\pi - \theta\right) + 1\right)\left(1 + \frac{2kh}{sinh\,(2kh)}\right) E(\sigma, \theta) d\sigma d\theta\right) \quad (6)$$

$$S_{xy} = S_{yx} = \frac{1}{2} g \left(\int_0^{2\pi}\int_0^{\infty} cos\left(\frac{3}{2}\pi - \theta\right) sin\left(\frac{3}{2}\pi - \theta\right)\left(1 + \frac{2kh}{sinh\,(2kh)}\right) E(\sigma, \theta) d\sigma d\theta\right) \quad (7)$$

{S}_{yy}=\frac{1}{2}g\left({\int }_{0}^{2\pi }{\int }_{0}^{\infty }\left({sin}^{2}\left(\frac{3}{2}\pi - \theta \right)+1\right)\left(1+\frac{2kh}{sin$h$\left(2kh\right)}\right)E(\sigma ,\theta)d\sigma d\theta \right) (8)

Where k is the wave number; h is the full water depth (m).

The local continuity equation in HD model is written as Eq. 9, and the two horizontal momentum equations for the x- and y- component are described as Eq. 10 and Eq. 11, respectively. Based on the hydrostatic approximation in vertical direction, the equation degenerated into Eq. 10:

$$\frac{\partial u}{\partial x}+\frac{\partial v}{\partial y}+\frac{\partial w}{\partial z}={S}_{HD} \quad (9)$$

$$\frac{\partial u}{\partial t}+\frac{\partial {u}^{2}}{\partial x}+\frac{\partial vu}{\partial y}+\frac{\partial wu}{\partial z}= fv-g\frac{\partial \zeta }{\partial x}-\frac{1}{{\rho }_{0}}\frac{\partial {p}_{a}}{\partial x}-\frac{g}{{\rho }_{0}}{\int }_{z}^{\zeta }\frac{\partial \rho }{\partial x}dz-\frac{1}{{\rho }_{0}h}(\frac{\partial {S}_{xx}}{\partial x}+\frac{\partial {S}_{xy}}{\partial y})+{F}_{u}+\frac{\partial }{\partial z}\left({\mu }_{v}\frac{\partial u}{\partial z}\right)+{u}_{s}{S}_{HD} \quad (10)$$

$$\frac{\partial v}{\partial t}+\frac{\partial {v}^{2}}{\partial y}+\frac{\partial uv}{\partial x}+\frac{\partial wv}{\partial z}= fu-g\frac{\partial \zeta }{\partial y}-\frac{1}{{\rho }_{0}}\frac{\partial {p}_{a}}{\partial y}-\frac{g}{{\rho }_{0}}{\int }_{z}^{\zeta }\frac{\partial \rho }{\partial y}dz-\frac{1}{{\rho }_{0}h}(\frac{\partial {S}_{yx}}{\partial x}+\frac{\partial {S}_{yy}}{\partial y})+{F}_{v}+\frac{\partial }{\partial z}\left({\mu }_{v}\frac{\partial v}{\partial z}\right)+{v}_{s}{S}_{HD} \quad (11)$$

$$\frac{\partial {p}_{a}}{\partial z}=-\rho g \quad (12)$$

Where t is time (s); \zeta is the water elevation (m), d is the still water depth (m), h=\zeta +d ; u ,v, w are velocity components in the x, y, and z directions, respectively (m/s); f is the Coriolis parameter (s^{-1}); \rho is the density of the water (kg/m^3) and {\rho }_{0} is the reference density (kg/m^3); {\mu }_{v} is the vertical eddy viscosity (m^2/s); {p}_{a} is atmospheric pressure (Pa); g is gravitational acceleration (m/s^2); {S}_{HD} is the source term and u_s and v_s are the velocity components at which the source water enters

the adjacent part. The terms of horizontal stress {F}_{u}, {F}_{v} can be described using the gradient stress, which is simplified to:

{F}_{u}=\frac{\partial }{\partial x}\left(2{\mu }_{h}\frac{\partial u}{\partial x}\right)+\frac{\partial }{\partial y}\left({\mu }_{h}\right(\frac{\partial u}{\partial y}+\frac{\partial v}{\partial x}\left)\right)	**(13)**
{F}_{v}=\frac{\partial }{\partial x}\left({\mu }_{h}\right(\frac{\partial u}{\partial y}+\frac{\partial v}{\partial x}\left)\right)+\frac{\partial }{\partial y}\left(2{\mu }_{h}\frac{\partial v}{\partial y}\right)	(14)

where {\mu }_{h} is horizontal eddy viscosity.
The surface (at z=\zeta, Eq. 6) and bottom (at z=-d, Eq. 7) boundary condition for u, v, w are determined by surface wind stress (\overrightarrow{{\tau }_{s}}) and bottom stress (\overrightarrow{{\tau }_{b}}):

\frac{\partial \zeta }{\partial t}+u\frac{\partial \zeta }{\partial x}+v\frac{\partial \zeta }{\partial y}-w=0, (\frac{\partial u}{\partial z},\frac{\partial v}{\partial z})=\frac{1}{{\rho }_{0}{\mu }_{v}}\overrightarrow{{\tau }_{s}}	**(15)**
u\frac{\partial d}{\partial x}+v\frac{\partial y}{\partial x}+w=0, (\frac{\partial u}{\partial z},\frac{\partial v}{\partial z})=\frac{1}{{\rho }_{0}{\mu }_{v}}\overrightarrow{{\tau }_{b}}	(16)

The stress is given by the following relation:

\overrightarrow{{\tau }_{s}}={\rho }_{a}{c}_{d}\left|{u}_{w}\right|{\overrightarrow{u}}_{w}	**(17)**
\overrightarrow{{\tau }_{b}}=\overrightarrow{{\tau }_{c}}+\overrightarrow{{\tau }_{w}}=0.5\rho ({f}_{c}\left|U\right|\overrightarrow{U}+{f}_{w}\left|{U}_{b}\right|\overrightarrow{{U}_{b}})	(18)
{U}_{b}=\frac{2{H}_{s}}{{T}_{z}}\frac{1}{sin$h$\left(2\pi h/L\right)}	(19)
L=\frac{g{T}_{z}^{2}}{2\pi }{\left(tan$h${\left[\frac{2\pi }{{T}_{z}}\sqrt{\frac{h}{g}}\right]}^{3/2}\right)}^{2/3}	(20)

Where {\rho }_{a} is the density of air (kg/m^3); {c}_{d} is the drag coefficient of wind depended on the wind speed; \overrightarrow{{u}_{w}} is the wind velocity (m/s); \overrightarrow{{\tau }_{c}} and \overrightarrow{{\tau }_{w}} are the shear stress induced by currents and waves, respectively; {f}_{c} and {f}_{w} are the current and wave friction factors determined by bed roughness {k}_{s}; U is the horizontal current velocity (m/s); {U}_{b} is the horizontal wave orbital velocity at the bed (m); L is the wave length (m).

The cohesive sediment transport was modeled using the Mud Transport module (MIKE 3 MT). The term of mud is generally used for fine-grained and cohesive sediment with grain sizes less than 0.063 mm. The module is based on the advection-dispersion equation:

\frac{\partial c}{\partial t}+u\frac{\partial c}{\partial x}+v\frac{\partial c}{\partial y}=\frac{\partial }{\partial x}\left({D}_{x}\frac{\partial c}{\partial x}\right)+\frac{\partial }{\partial y}\left({D}_{y}\frac{\partial c}{\partial y}\right)+\frac{\partial }{\partial z}\left({D}_{z}\frac{\partial c}{\partial z}\right)+{S}_{MT}+{S}_{E}+{S}_{D}	(21)

Where c is the SSC (kg/m^3); {D}_{x}, {D}_{y}, and D_z are dispersion coefficients (m^2/s); {S}_{MT} is source term; {S}_{D}, {S}_{E} are the deposition and erosion terms (kg/m^3/s). The deposition rate {S}_{D} can be expressed by Eq. 22, and the erosion rate for dense, consolidated bed and soft, partly consolidated bed are defined by Eq. 23 (Partheniades 1965) and Eq. 24 (Parchure and Mehta 1985), respectively:

$$S_D = w_s c_b \left(1 - \frac{|\overrightarrow{\tau_b}|}{\tau_{cd}}\right) \quad (22)$$

$$S_E = Q\left(\frac{|\overrightarrow{\tau_b}|}{\tau_{ce}} - 1\right)^n \quad (23)$$

$$S_E = Qexp\left[\alpha(\tau_b - \tau_{ce})^{1/2}\right] \quad (24)$$

Where {w}_{s} is the settling velocity of each sediment fraction (m/s); {c}_{b} is the near bed concentration (kg/m^3) that proportional to c; {\tau }_{cd} and {\tau }_{ce} are the critical shear stress for deposition and erosion (N/m^2); Q is the erodibility of bed (kg/m^2/s); n and \alpha are the power of erosion for dense and soft bed, respectively. Additionally, the dry density of the bed {\rho }_{b} is also needed to refresh the bed thickness during calculating.
The MIKE 3 model solves the integrated equations of mass conservation and momentum conservation in space and time by using explicit and implicit alternating techniques. The solution of each direction and individual grid are achieved applying double precision scanning method.

2.3.2 Grid generation

To simulate the hydrodynamic and sediment action of Lake Taihu by the MIKE 21/3 model, determining the exact bathymetric data of the lake was considered the most basic step. The water depth (z) data was obtained from the work of Qiu et al. (2013), a measurement in 2009 covering 69×69 sampling points of the whole lake. The xyz file for land area was created then and fed as input to MIKE 21/3 software to calculate depth contours for model domain. As shown in Fig. 1, the lake center has the largest depth of 2.4m, while the east part is relative shallow.

Unstructured triangle grid was created by mesh generator module in MIKE zero. In the horizontal direction, nested grid was adopted by applying Triangulation parameters with maximum element area of 400000 m^2 and maximum number of nodes 100000 for the regional model (the whole lake). Local model zooming on the area around the water intake with maximum element area 80000 m^2, the minimum side length of the grid was approximately 100 m. In this way, the boundaries of local model are given by the corresponding calculated data from the regional model, which can make the simulation results more accurate. σ-average layer was used in the vertical direction. Because of the shallowness of the lake, 5 uniform layers were considered adequate to resolve the structures. Imported bathymetric values were then interpolated to cover each grid and mesh. The finally developed mesh consisted of 51275 non-overlapping elements, 33036 nodes.

2.4 Calibration

Before application, the model was calibrated by modifying the coefficients empirically or through measurements to fit the situation of the study area. For the lack of field measurements which are supposed to cover the entire lake, results from the work of Zhao Q. et al (2018) was referred to calibrate and get the best performance of the developed model in this paper. They simulated the flow, wave height and sediment concentration distribution of Lake Taihu under stead wind action (SW wind of 9m/s and 12m/s) by the MIKE DHI software, a similar method as current study.

For the HD module, there are 3 main influencing coefficients: the (horizontal/vertical) eddy viscosity coefficient, the bed resistance coefficient, and the wind friction coefficient. The horizontal and vertical eddy viscosity were determined through the Smagorinsky formulation and constant eddy formulation, respectively. The coefficients in previous work varied widely with a range of 0.001~ 5 (Shu et al. 2021; Tang et al. 2011), and the determined values of 0.28 for horizontal and 0.3 for vertical were obtained to be optimal finally. The bed resistance was described by Manning number here and set as a constant of 31 $m^{1/3}/s$ in domain after calibration. Wind friction coefficient varied linearly with wind speed, high values often leads to good performance with strong winds, whiles for weak winds, smaller coefficients should be used, the default values were adopted here. The initial surface elevation was set as 0 m for all working conditions, that is, the initial water depth was equal to the bottom elevation. Since the water level of Lake Taihu has a small fluctuation within 30cm (Xu et al. 2020), it was reasonable to leave out the impact of it on sediment distribution. The SW model operates based on fully spectral formulation to achieve wind-waves growth, and the most influential factor, bottom friction, was expressed by Nikuradse roughness, which was 0.03 according to the model performance. The limitation of wave frequency and wave breaking coefficient were set as default, and the influence of white capping was ignored due to the relative weak effect in shallow water body.

The hydrodynamic information from the HD and SW simulations were directly used in the MT model. For this part, the sediment parameters set in MT model was closely related to the simulation results, including number of bed layers and sediment fractions, settling velocity, critical shear stress, density and thickness of layers, and so on. These parameters were referred to the previous works conducted in Lake Taihu. Qin et al (2007) investigated the spatial distribution of sediments at 723 sites, and found that sediment covers about 45% of lake area with a depth of 0.6~5.5 m, mass exchange in the water-sediment interface exists mainly within the top 5~10 cm (Qin et al. 2004; Luo et al. 2004). And the unconsolidated sediment was mainly concentrated in the northwestern and southeastern sections (and) of the lake, whereas the consolidated sediment was primarily confined to the central region ( ) which was frequently disturbed by wind induced waves (Wu et al. 2018). Thus, 2 bed layers were set in the MT model, with a constant thickness of 0.1 m for the weak fluid mud layer (layer1) and spatial varying for fluid mud layer (layer2, Online Resource1). The dry density of bed material were180 and 320 kg/m^3 respectively according to geological property. The primary parameters for erosion process occurred at bottom layer were erosion coefficient and critical shear stress, which were taken as 0.02 N/m^2, 0.00002 for layer1 and 0.05, 0.0001 for layer2 on the basis of previous studies (Luo et al. 2004). Works of the spatial distribution of sediments granulometric composition conducted in Lake Taihu revealed that, the particle size ranged in

0.002 ~ 0.14 mm, sediments with particle sizes below 0.02 mm (i.e., silt and clay) accounted for approximately 80% (Hu et al. 2006; Hou et al. 2013). Therefore, the sediments was divided into 2 fractions, and the critical shear stress and mean settling velocity controlling the deposition process were 0.03 N/m^2, 0.00002 m/s for fraction1 and 0.05 N/m^2, 0.0008 m/s for fraction2 (Qiu et al. 2013; Pang et al. 2006).

The comparison between the modeling results by the effect of SW wind (9m/s) was shown in Online Resource2, the agreement of them was satisfied in general, especially for current speed and significant wave height. With strong winds, flows formed parallel to the shore acquired good speed that higher than 0.08m/s, and the central region followed with speed of above 0.04m/s. Narrow areas such as East Taihu Bay (□), Meiliang Bay (□) and Xukou Bay (□) shared relative slow currents that below 0.02m/s, which was attributed to the calm condition with significant wave height lower than 0.16m. The largest wave height (larger than 0.32m) had occurred at the central area due to the wide air-water interface and deep water depth, the activated wave action enabled great current speed to carry sediment and responded with high SSC then. Miner discrepancy in sediment distribution was observed, according to Zhao, J., et al.'s work (2018), the region of East Taihu Bay (□) stood out with SSC values higher than 0.16kg/m^3, and particles deposit at the East zone (□) and Gonghu Bay (□) as well. However, the results of current study acquired maximal SSC of above 0.1kg/m^3 at the central part (□) of the lake. This may attribute to the setting of layer thickness, Zhao et al (2018) adopted a uniform sediment layer, whereas the current model considered spatial discrepancy. Heavy unconsolidated bed layer near the Xishan Island made a great deal of sediment conveyed to the center during southwesterly wind events, consequently engendered higher concentration at the northern than the East Taihu Bay (□). The primary parameters determined after calibration were summarize as Online Resource3.

3 Working Conditions Setting

Wind field data have been processed through classification, wind speed was separated into 12 intervals from 0~ 12 by increments of 1m/s and larger than 12 m/s, and wind directions was divided into 16 intervals. The seasonally characteristics of the wind field were also considered, 5 windrose diagrams were displayed in Fig. 2, each was characterized by frequencies appearance, and labels close to the petals showed the mean wind speed of sub dataset within this part. The wind direction was also presented by onshore, offshore and alongshore according to the direction of shoreline of water intake area.

For the year 2020, there were 4 main wind directions (ESE, SE, SSE, NNW) accounting for 38.1% (9.9%, 10.4%, 8.9%, 8.9%, respectively) with mean speed of 2.4m/s, 1.8m/s, 2.0m/s, 4.8m/s, and followed by S (7.7%), NW (7.7%), NE (7.0%), E (7.0%), N (6.8%), NNE (6.7%). The median speed was about 3m/s, for the interval of 0~3m/s occupied 54.7% of all samples, and 98.3% were below 8m/s. More precisely, most of the strong winds were found in onshore winds (WNW, NW, NNW) which contributed 20.8% of the year. Whereas weaker winds were strongly related to offshore wind directions (ESE, SE, SSE), which accounted for 29.1%. The characteristics of the winds of the study area provided diversification from one season to

another. During winter, onshore winds with average speed of 4.3 ~ 4.9m/s primarily prevailed over Lake Taihu, the dominant wind was in the NNW direction associated with relative strong force. As for summer, offshore winds was leaded with average speed of 2.0 ~ 2.7m/s, the main wind of SSE was characterized by low speed. For the other months, the wind fields seemed to be less concentrated, since multi dominant wind directions were found during this period. In spring, the winds came from the east and south with mean speeds varying principally between 1.6 and 2.9 m/s. The winds in fall were mostly northerly, with mean speeds ranging from 3.3 to 4.7 m/s.

Overall, the wind fields at Lake Taihu were changefully with the speed from clam (<0.1m/s) to a maximum of 13.2m/s, and the wind directions were scattered as well. Therefore, 192 models driven by wind forces covering all regimes (12 speed-intervals of 1m/s and 16 direction-intervals, cases of wind speed >12m/s were neglected for the extreme low proportion, which accounted only 0.15% of all samples) were built up to achieve a comprehensive investigation of sediment dynamics behavior under diversiform wind conditions at the water intake area. Considering that the water intake area is shield from southeasterly winds but exposed to long fetch for winds from the north or west, typically cases of onshore (NNW), offshore (SSE) and alongshore (ENE and WSW) winds at 3m/s and 8m/s were taken as analysis objects to detailed observe both the combine and separate effect of wind speed and direction on sediment distribution of the lake.

4 Results And Discussion

4.1 The effect of wind fields on sediment distribution

As shown in Fig. 3a and Fig. 4a, the final stable wind-current distributions were the combination of circulations and alongshore currents. The patterns of inversed winds displayed extremely similar but with inversed rotation gyres, which resulted from the bottom topography (Luo et al. 2003). The current speed increased sharply in occurred in response to the enhance of wind force. Generally, the alongshore currents paralleling to the wind direction acquired relative high speed since less energy has been absorbed by boundaries, and semi-closed bays obtained extremely calm flow correspondingly. Circulations were subject to form at the lake shores, with counter-clockwise gyres mainly generated at the windward shores, whereas reverse ones were more likely to generate at the leeward. For the NNW and SSE winds (Fig. 3a), the maximum flow rate displayed at the southwest shore for the long lake shoreline over 20km with about 0.02m/s and 0.1m/s at the wind speed of 3m/s and 8 m/s, respectively. When the lake went through WSW and ENE winds, the highest values (about 0.03m/s and 0.09m/s at the wind speed of 3m/s and 8 m/s, respectively) occurred at the narrow areas before the mouth of the Xukou Bay.

Wind-waves grew higher following the increase of wind force as well, with greater friction drag delivering more energy into the water through turbulence and then dissipated by bottom friction. The propagation direction of the wind-waves was almost consistent with the wind direction (Fig. 3b, Fig. 4b). Waves increased from the windward shoreline to the open water, being much higher than those at leeward shores when less wind energy (at the wind speed of 3m/s) was conveyed into water. Contributing to this

is that the significant wave height was induced by water level oscillations and their distribution patterns are related to the wind fetch (the horizontal distance that wind continues to blow across the water surface). Long fetch helped to wave growth, and wind speed significantly impacts the wave motion in the lake (Zheng et al. 2015). However, waves achieved fun growth when the wind speed reached 8m/s, central region obtained largest wave height (above 0.32m) then because of the relative wide surface and deep depth.

Overall, onshore strong winds can effectively activate higher wave shear stress, whereas lower offshore winds contributed less in it's generation (Fig. 3c, Fig. 4c). Once the threshold stress is exceeded, sediment particles can be triggered and enter the overlying water body, thus leads to the increase of SSC values. Contrariwise, waves are of low energy with very low suspension potential. The corresponding sediment fields were presented in Fig. 3d and Fig. 4d, it can be seen that wind direction has a pronounced influence on sediment dispersal. It determined the direction and efficiency of the propagation, whereas wind strength affected the spatial intensity. Analogous patterns of shear stress and SSC at the wind speed of 3m/s within the same direction may ascribe to the particularly low potential of sediment transportation. With a light wind, the shear stress induced by waves ranged from 0 to 0.06 N/m^2 and was below 0.01 N/m^2 at most area, which was lower than the critical value triggering sediment resuspension (Li 2016; Qin 2004; Luettich R.A. et al. 1990). That made less particles suspended and thus transportation played a negligible role in sediment redistribution. As wind speed increasing, more energy was delivered to hydrodynamic processes (waves and currents), the shear stress distribution went through microscale to the entire lake and the critical shear stress at the upper limit of 0.06kg/m^3 (with the range of 0.02~0.06 kg/m^3 indicated by previous studies) was exceed for almost the whole area. Deviations between shear stress and sediment patterns were observed then, especially at the central region.

Due to the short distance between water intake and lake shore, the local SSC was impacted significantly by the resistance from the shore in particular with the typical condition of onshore (NNW) and offshore (SSE) winds. The water intake area was exposed to long fetch and suffered from high waves in the case of NNW winds, the activated waves efficiently motivated the sediment and promoted particle entrainment. Since the abundant lakebed deposits at the southeastern part of the lake enabled sediment easily to enter the overlying water body by the wave disturbance, particles suspended at that area were then conveyed into the observed site along with the southeastern wind-currents. Both the effect of suspension and transportation helped to develop high SSC when the lake went through northwesterly winds, which caused the low incipient wind speed (< 3m/s) for SSC increase at the water intake area. And the circulation formed here by the resistance of the lakeshore hindered movement and deposition of the suspended sediment, providing the conditions for maintenance of high SSC values. A similar process was appeared under SSE winds, which led to high SSC at the northwestern shore of East Taihu Bay and northwestern section of the lake (and), but extremely low SSC values at the study site instead.

By the effect of alongshore winds, the southeastern lake was confronted by short wind fetch that was adverse to the development of waves. The tiny shear stress generated at the site by the wind speed of 3m/s failed to trigger deposits, thus higher energy was required for incipient motion of SSC increase

compare to northwester wind. As most regions achieved the critical shear stress in response to the increased wind force, the sediment was stimulated. Suspended particles at the East Taihu Bay (□) moved towards the water intake area firstly by ENE wind, and the followed inverse compensating currents carried sediment from the littoral zone (□) to the site then, consequently caused increase of SSC. Approximate progress was developed in the condition of WSW wind, sediment was transported from the littoral zone at first and then the Bay instead. Seeing that the observed site was at the mouth of the Bay and a large amount of sediment was directly transported here, the local SSC may be higher than that under onshore conditions with the same wind speed.

The steady values of simulated SSC at the water intake under different model conditions was described in Fig. 5. In all, the sediment concentration varied with large amplitude by different wind events, and the incipient speed for sediment motion was disparate among wind directions. Onshore winds (NW, N, NNW, WNW) were more subjected to enhance local SSC that speed above 2 m/s was sufficient to evoke sediment behavior. Comparably, offshore winds (SE, S, SSE, ESE) were weak in increasing SSC of the site, slight ascent could be observed only when wind speed reached over 5m/s. For alongshore winds, sediment was activated when the speed was greater than 4m/s.

The processes of sediment dynamics of the water intake can be approximately illustrated by 3 stages based on 2 wind speed thresholds: (1) within the speed range of 0~3m/s, fewer sediment was activated or transported into the observed site, indicating a relative calm circumstance of the entire lake, and onshore winds played a controlling role in SSC rising, while alongshore winds began to take effect later this stage; (2) as the speed went up and was below 8m/s, the sediment bed was triggered and the SSC in the study site went up gradually (0.02~0.1 kg/m^3) along with wind speed, and alongshore winds acted more powerful than onshore ones in this stage; (3) prodigious increase of SSC occurred (0.1~0.8kg/m^3) once the wind speed was above 8 m/s, a large amount of sediment was suspended, and complex migration came up due to the dramatic hydrodynamic behavior as well.

4.2 The prediction of turbidity based on simulation model

The simulated SSC values in the water intake area were matched to the measured turbidity according to the recorded wind conditions with linear interpolation (Eq. 25), to observe the relationship between the two series:

$$\{S\}_{c(i,j)}=\left(\{S\}_{\left(i\text{'},\lceil j\rceil\right)}-\{S\}_{(i\text{'},\lfloor j\rfloor)}\right)\bullet (j-\lfloor j\rfloor)+\{S\}_{(i\text{'},\lfloor j\rfloor)} \quad (25)$$

Where i and j were the hourly wind direction and wind speed recorded by meteorograph at the Pulou station; i\text{'} was the direction interval that i located in among 16 wind directions; $\lfloor j\rfloor$ and $\lceil j\rceil$ were the floor and ceiling of j, and met the condition of $0 \le \lfloor j\rfloor \le \lceil j\rceil \le 12$m/s; {S}_{c(i,j)} was the calculated hourly SSC of the wind condition (i,j); {S}_{(i,j)} was the simulated SSC at the working condition (i,j).

The pattern model representation (PMR) was then introduced to measure the trend similarity of the time series (Wang et. al. 2004), it is based on piecewise linear representation and overcomes the problem of time series mismatch based on point distance. According to the numbers of segmentations, series pattern distance (SPD) calculated by different scale features reflects the different similarities of series, and a pattern represents one segment monotone's tendency. In this paper, the pattern was defined as triple, that was {up, hold, down}, and was represented as P = {1,0,-l} correspondingly to facilitate calculation. Let L = ({l}_{1}, {l}_{2},..., {l}_{i}) be a time series, the element of the pattern set p ϵ P, was marked by introducing the amplitude threshold \sigma:

$$p = \begin{cases} 1 & when\ (l_i - l_{i-1})/l_{i-1} < -\sigma \\ 0 & when\ |(l_i - l_{i-1})/l_{i-1}| \le \sigma \\ -1 & when\ (l_i - l_{i-1})/l_{i-1} > \sigma \end{cases} \quad (26)$$

The time series of {S}_{c} and T were finally transformed as order sets of the (pattern value, time stamp) pair:

{S\text{'}}_{c}=\left[\right({p}_{{S}_{c}}\left(1\right), {t}_{1}),...,({p}_{{S}_{c}} \left(n\right), {t}_{n}\left)\right]	**(27)**
T\text{'}=\left[\right({p}_{T}\left(1\right), {t}_{1}),...,({p}_{T}\left(n\right), {t}_{n}\left)\right]	(28)

Where {S\text{'}}_{c} and T\text{'} were the pattern series of {S}_{c} and T; {t}_{i} was the time phase; {p}_{{S}_{c}}\left(i\right) and {p}_{T}\left(i\right) were the pattern elements of the two series keeping from {t}_{i-1} to {t}_{i}. The pattern distance (D) was calculated as Eq. 29:

$$D=\frac{1}{N}({({p}_{{S}_{c}}\left(i\right)-{p}_{T}\left(i\right))}^{2} \quad (29)$$

Where N is the number of pattern segments.

Considering that the error of turbidity prediction varied from 5% to above 20% according to existing researches, the variation amplitude threshold \sigma for pattern model representation was selected as 0.05 and 0.2 in this study. The quantified similarity of the hourly trends of calculated SSC and turbidity (Fig. 6) showed that the two temporal sets were synchronous for approximately 40% of all conditions and get a pattern distance of 1.12 according to Eq. 28 when \sigma was 0.05, for \sigma =0.2, the frequency of D = 0 and the pattern distance was 50.9% and 0.70 respectively. Since SSC was a short-term response parameter, which replied slowly to the wind condition rather than complete synchronization, the temporal trend of it and turbidity was less synchronous as well due to the lag reaction of sediment resuspension and transportation, and the lag time frame also reflected the water-column residence time of sediments resuspended by wind generated wave activity. The pattern distance of 0 to 23 lag hours was considered in this paper to find the optimum lag frame of the study area (Fig. 6), and the state of 9-hour lag gets the best performance for all conditions. Owing to the 2-hour delay to pump raw water from the intake area to the waterworks, 7-hour lag was believed as the optimal state for the current study. The result was conform to the existing research results (Zhao et. al., 2018) that the lag phase varying from 2 to 10 depending on local conditions. The lowest distance and the highest proportion of synchronous cases decreased to 0.85 and increased to 48.2% at \sigma =0.0.5, 0.55 and 64.1% for \sigma =0.2, respectively.

The {S}_{c} calculated according to Eq. 26 and the turbidity series were all managed as day-mean ones to weaken the interference of extreme values. The time series of {S}_{c} and 7-hour-lag turbidity seemed to coincide with each other satisfactorily, especially at peak values (Fig. 7). Hhigher values were all more subjected to occurred during winter, which was characterized by typical onshore (northwesterly) winds with high speed. This could be used to further confirm that the strong wind force of northwestern and the induced waves and currents were readily loosened the sediment structure and stimulated particles to resuspend and migrate for the long fetch and consequently considerable energy, thus effectively developing turbidity maximum at the water intake.

The high similarity of modeling SSC and measured turbidity confirmed the reasonability of simulation results and manifested that the turbidity of the study area was strongly related to sediment particles. However, it should be also noticed that distinguished discrepancies were presented during January and from September to November. For the former, the turbidity was distinctly the largest among the whole year but the value of SSC kept approximate to other months, while the two items shared extremely similar tendency. The relatively high concentration of cyanobacteria (Online Resource 4) may engender this deviation since the aggregation of the alga made the background turbidity boost which was insensitivity to the wind condition. Similar phenomenons can be observed in May and December as well with comparatively inconspicuous states. For the period of September to November, the SSC fluctuated remarkably while the turbidity kept relatively low and steady, this may attribute to the wind condition which was characterized by multi-prevailing directions (Fig. 2). Since the process of wind energy transfer was time-consuming that only winds in a specific situation acted continuously on the water surface enabled significant wave heights, thus increasing friction drag between air and the water surface and ultimately activating sediment motion. The simulated SSC used in the analysis was conducted from models reaching stability, however, the polytropic winds failed to achieve it in actual circumstances that caused the deviation.

The results manifested that the model was prospective to predict the tendency of raw water turbidity according to weather forecast. For the precise prediction of hourly weather condition has achieved a advance of 1-3 days nowadays, the current model was supposed to foresee the general variation of turbidity with a same time span. The reserved time was crucial for waterworks to adjust the operation parameter, correspondingly improve the efficiency for management.

5 Conclusions

The current study investigated the effect of wind forces on hydrodynamic and sediment distribution of Lake Taihu based on field simulation and further observed the sediment source at the water intake area under typical wind conditions. Generally, areas exposed to long wind fetch were more subjected to activate hydrodynamic behavior, leading to intensive resuspension. By the effect of typical onshore (NNW) winds, sediment transported from the central region and suspended at the local area together contributed to the high SSC at the water intake, whereas the East Taihu Bay and the littoral zone were the main suppliers for the case of alongshore (WSW and ENE) winds. Offshore (SSE) winds could hardly

promote sediment motion at the leeward bank, thus resulting in extremely low SSC at the site. The analogical temporal series of modeling SSC and measured turbidity with 7-hour-lag proved the feasibility and effectiveness of the simulation model in turbidity prediction. The study applied field simulation on site investigation that enabled a more comprehensive acknowledge of sediment behavior at observation site by considering redistribution of particles in space and lag reaction of wind force in time.. In addition, the work provided an idea for turbidity prediction of waterworks sharing similar environmental conditions (i.e., the water source area is sensitive to wind changes and the turbidity is mainly caused by sediment behaviors). However, the model was only an approximate representation of the actual turbidity, further study about the quantitative relationship between simulated SSC and measured turbidity is required to achieve a more definitive forecast. And attention also should be paid on the measurements of reducing the turbidity in water intake area based on current work.

Declarations

Acknowledgements :

This work was financially supported by the National Science and Technology Major Projects for Water Pollution Control and Treatment (No. 2017ZX07201003).

Funding:

This work was financially supported by the National Science and Technology Major Projects for Water Pollution Control and Treatment (No. 2017ZX07201003).

Author Contributions:

Xinyu Yao: Methodology, Validation, Formal analysis, Writing - Original Draft; Xiaowei Liu: Project administration, Writing - Review & Editing; Yongchao Zhou: Project administration, Writing - Review & Editing; Liang Zhang: Resources, Data Curation; Zhixu Zhou: Resources, Data Curation; Yiping Zhang: Conceptualization, Writing - Review & Editing, Supervision.

Ethics approval:

All the sources have been cited appropriately and thereis no such issue during thisstudy.

Consent to participate:

All the authors will participate in review andpublication process.

Consent to publish:

All the authors have given their consent to publishthis study.

Competing Interests:

The authors have no relevant financial or non-financial interests to disclose.

References

1. Aani SA, Bonny T, Hasan SW, Hilal N(2019) Can machine language and artificial intelligence revolutionize process automation for water treatment and desalination ? Desalination 458: 84-96.https://dx.doi.org/10.1016/j.desal.2019.02.005
2. Bohling B(2009)Measurements of threshold values for incipient motion of sediment particles with two different erosion devices.J Marine Syst 75:330–335.https://doi.org/10.1016/j.jmarsys.2007.01.014
3. Burchard-Levine A, Liu SM, Vince F, Li MM, Ostfeld A,(2014) A hybrid evolutionary data driven model for river water quality early warning. J Environ Manage 143: 8–16.https://dx.doi.org/10.1016/j.jenvman.2014.04.017
4. ChaoX, JiaY, ShieldsFD, WangS, CooperCM (2008) Three-dimensional numerical modeling of cohesive sediment transport and wind wave impact in a shallow oxbow lake. Adv Water Resour 31:1004–1014.https://dx.doi.org/10.1016/j.advwatres.2008.04.005
5. Hasselmann K, Barnett TP, Bouws E, et al(1973) Measurements of wind-wave growth and swell decay during the Joint North Sea Wave Project (JONSWAP). Dtsch Hydrogr Z 8: 1–95.https://doi.org/10.1093/ije/27.2.335
6. Hou J,Wang C, Wang PF, Qian J(2013) Temporal variability and spatial distribution of granulometric composition ofsurface sediments and classification in Taihu Lake. J Hohai Univ (Nat Sci) 41:114–119.https://doi.org/10.3876/j.issn.1000-1980.2013.02.004 . (in Chinese)
7. Hu CH, Hu WP, Zhang FB, et al(2006) Sediment resuspension in the Lake Taihu, China. Chinese Sci Bull 51:731–737.https://doi.org/10.1007/s11434-006-0731-2
8. Jalil A,Li YP, Zhang K, et al (2019) Wind-induced hydrodynamic changes impact on sediment resuspension for large, shallow Lake Taihu, China. Int J Sediment Res 34: 18–28. https://doi.org/10.1016/j.ijsrc.2018.11.003
9. Jin KR, Ji ZJ(2001) Calibration and verification of a spectral wind–wave model for Lake Okeechobee. Ocean Eng 28:571–584.https://doi.org/10.1016/S0029-8018(00)00009-3
10. Kennedy MJ, Gandomi AH, Miller CM, (2015) Coagulation modeling using artificial neural networks to predict both turbidity and DOM-PARAFAC component removal. J Environ Chem Eng 3:2829–2838.http://dx.doi.org/10.1016/j.jece.2015.10.010
11. Kessarkar PM, Rao VP, Shynu R, et al (2009)Wind-driven estuarine turbidity maxima in Mandovi Estuary, central west coast of India. J Earth Sys Sci 118: 369–377. https://dx.doi.org/10.1007/s12040-009-0026-5
12. Komen GJ, Caveleri L, Donelan M, et al(1994) Dynamics and Modelling of Ocean Waves. Dynam Atmos Oceans 25:276-278.https://doi.org/10.1016/0377-0265(95)00469-6

13. Kuang C, Wang YB, Gu J, Lei G(2016) Study of hydrodynamics using a bi-directional wave-current coupled model in Haitan Bay, Fujian province. J Tongji Univ (Nat Sci) 8: 1212–1220. https://doi.org/10.11908/j.issn.0253-374x.2016.08.011. (in Chinese)
14. Kumagai M(1988) Predictive model for resuspension and deposition of bottom sediment in a lake.Jpn J Limnol 49:185–200.https://doi.org/10.3739/rikusui.49.185
15. Li YP, Tang CY, Wang JW, et al(2016) Effect of wave-current interactions on sediment resuspension in large shallow Lake Taihu, China. Environ Sci Pollut Res 24: 4029–4039.https://doi.org/10.1007/s11356-016-8165-0
16. Luo LC, Qin BQ, Zhu GW(2004)Sediment distribution and the maximun resuspension depth with disturbance in Lake Taihu[J]. J Sed Res 1: 9–14.https://doi.org/CNKI:SUN:NSYJ.0.2004-01-001 . (in Chinese)
17. Luo LC, Qin BQ(2003) Numerical simulation based on a three-dimensional shallow-water hydrodynamic model in Lake Taihu -Current circulations in Lake Taihu with prevailing wind-forcing[J]. J Hydrodyn 18() 686–691. (in Chinese)
18. Luettich RA, Harleman DR, Somlyody L(1990)Dynamic behavior of suspended sediment concentrations in a shallow lake perturbed by episodic wind events. Limnol Oceanogr35:1050–1067. https://doi.org/10.4319/lo.1990.35.5.1050
19. Pang Y, Li YP, Luo LC(2006) Study on the simulation of transparency of Lake Taihu under different hydrodynamic conditions. Sci China: Ser D 49: 162–175. https://doi.org/10.1007/s11430-006-8116-6
20. Parchure T, Mehta A(1985) Erosion of Soft Cohesive Sediment Deposits. J Hydraul Eng 111:1308-1326.https://doi.org/10.1061/(ASCE)0733-9429(1985)111:10(1308)
21. Partheniades E(1965) Erosion and Deposition of Cohesive Soils. Am Soc Civ Eng 91:190-192.https://doi.org/10.3109/15622970109026808
22. Qin BQ, Hu WP, Gao G, Luo LC, Zhang JS(2004) Dynamics of sediment resuspension and the conceptual schema of nutrient release in the large shallow Lake Taihu, China. Chinese Sci Bull 49:54–64.https://doi.org/10.1007/BF02901743
23. Qin B, et al(2005)Models and estimation methods of endogenous nutrient release from sediments of large shallow lakes: A case study of Taihu Lake. Sci China Ser D 49:38–50. https://dx.doi.org/10.3969/j.issn.1674-7240.2005.z2.004 . (in Chinese)
24. Qin BQ, Xu PZ, Wu QL et al(2007) Environmental issues of Lake Taihu, China. Hydrobiologia 581:3–14.https://doi.org/10.1007/s10750-006-0521-5
25. Qiu H, Zhao QH, Zhu WJ(2013) Model simulation of suspended solids in taihu lake under real meteorological condition. Oceanologia et Limnologia Sinica 44: 1418–1426.https://dx.doi.org/CNKI:SUN:HYFZ.0.2013-06-002 . (in Chinese)
26. Sheng Y, LickW, (1979) The transport and resuspension of sediments in a shallow lake. J Geophys Res84:1809–1826. https://dx.doi.org/10.1029/JC084iC04p01809

27. Shu YH, Gao CC, (2021) Numerical simulation of wind-driven current and pollutant transport and diffusion in Taihu Lake. Water Resour Prot37: 121–127.https://dx.doi.org/10.3880/j.issn.1004-6933.2021.02.019 . (in Chinese)
28. Stone R(2011) China aims to turn tide against toxic lake pollution. Sci (New York, N.Y.) 333:1210–1211. https://dx.doi.org/10.1126/science.333.6047.1210
29. Tang CY, Li YP, Acharya K, et al(2019) Impact of intermittent turbulent bursts on sediment resuspension and internal nutrient release in Lake Taihu, China. Environ Sci Pollut Res26: 16519–16528.https://dx.doi.org/10.1007/s11356-019-04847-2
30. Tang CY, Li YP, He C, Acharya K(2020) Dynamic behavior of sediment resuspension and nutrients release in the shallow and wind-exposed Meiliang Bay of Lake Taihu. Sci Total Environ 708:135131.https://dx.doi.org/10.1016/j.scitotenv.2019.135131
31. Tang LL, Wang P, Yao Q (2011) Three-dimensional numerical simulation of current, waves and sediment transportin Taihu Lake. Water Resour Prot 27:1–5.https://dx.doi.org/10.3969/j.issn.1004-6933.2011.02.001 . (in Chinese)
32. Wang D, Rong G (2004) Pattern distance of time series. J Zhejiang Univ (Eng Sci) 29: 53–61. https://dx.doi.org/10.1007/BF02873091
33. Wang JD, Qi WG(2009) Prediction of River Water Turbidity Based on EMD-SVM. Acta Electronica Sinica 37: 2130–2133.https://dx.doi.org/10.1016/j.apm.2007.10.019 . (in Chinese)
34. Wu TF, Qin BQ, Zhu GW et al (2013)Modeling of turbidity dynamics caused by wind-induced waves and current in the Taihu Lake. Int. J Sed Res 28: 139–148.https://dx.doi.org/10.1016/S1001-6279(13)60026-8
35. Wu TF, Qin BQ, Brookes D, et al(2018) Spatial distribution of sediment nitrogen and phosphorus in Lake Taihu from a hydrodynamics-induced transport perspective. Sci Total Environ 650:1554–1565.https://dx.doi.org/10.1016/j.scitotenv.2018.09.145
36. Xu RC, Pang Y, Hu ZB, Zhu TY(2020) Relationship between water age and hydraulic residence time in Taihu Lake and parameter sensitivity. Water Resour Prot 36: 38–43. http://dx.doi.org/10.3880/j/issn.1004-6933.2020.03.007 . (in Chinese)
37. Zhang P, Chen XL, Lu JZ, Zhang W(2015) Assimilation of remote sensing observations into a sediment transport model of China's largest freshwater lake: spatial and temporal effects. Environ SciPollut Res https://dx.doi.org/10.1007/s11356-015-4958-9
38. Zhao JJ, Wei ZP, Liu J, (2018) Numerical simulation of hydrodynamic force to suspended sediment of Taihu Lake. Port Waterway Eng 550:119–125.https://dx.doi.org/10.16233/j.cnki.issn1002-4972.20181205.008 . (in Chinese)
39. Zhao QH, Chen SQ, Chen SY(2018)Turbidity in response to wind speed, wind direction and wind duration in Gonghu Bay, Lake Taihu. J Lake Sci30:1587–1598.https://dx.doi.org/10.18307/2018.0610 . (in Chinese)
40. Zheng SS, Wang PF, Wang C, Hou J(2015) Sediment resuspension under action of wind in Taihu Lake, China. Int J Sed Res 30: 48–62. https://dx.doi.org/10.1016/S1001-6279(15)60005-1

Figures

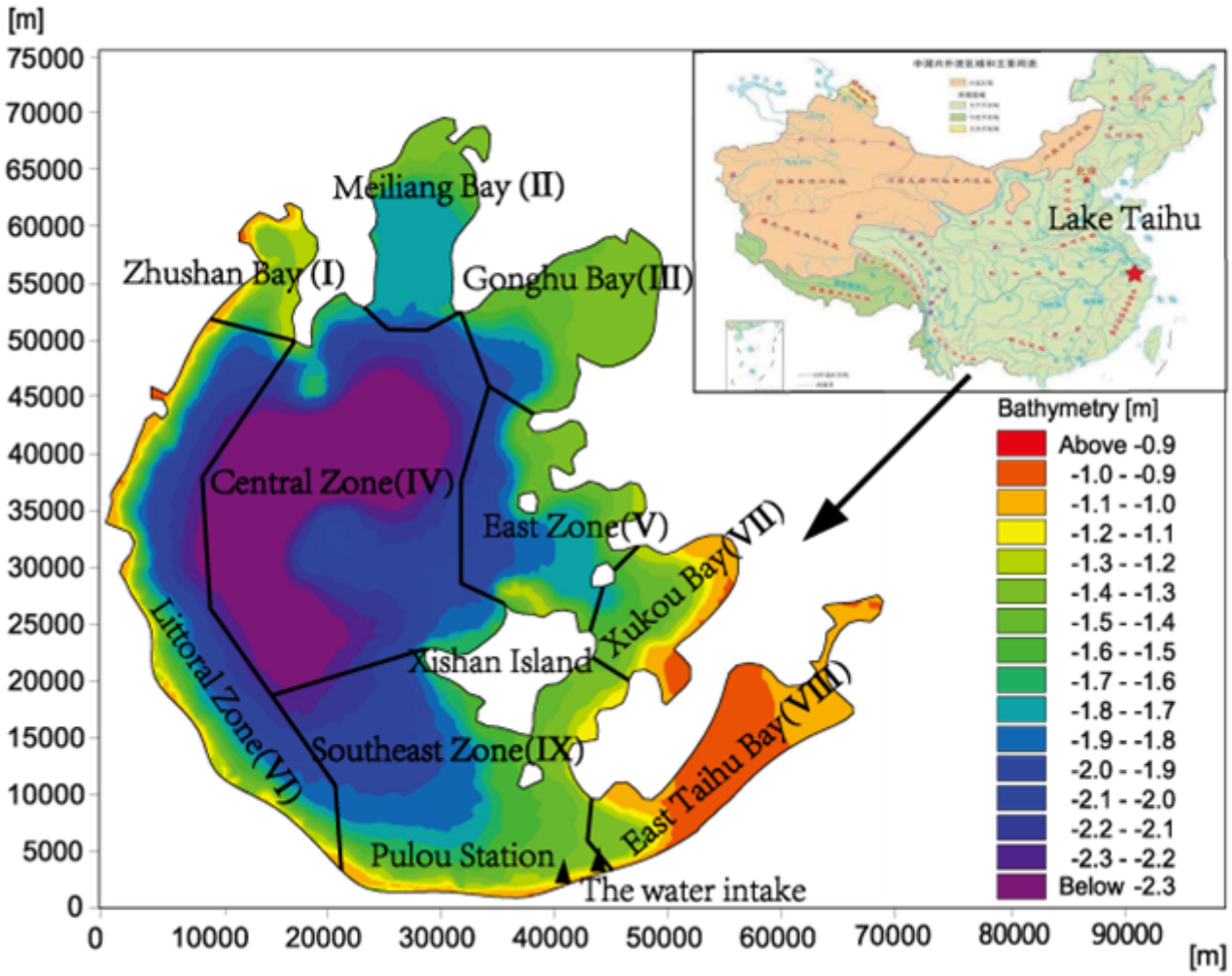

Figure 1

Location and Bottom elevation of Lake Taihu with observation site

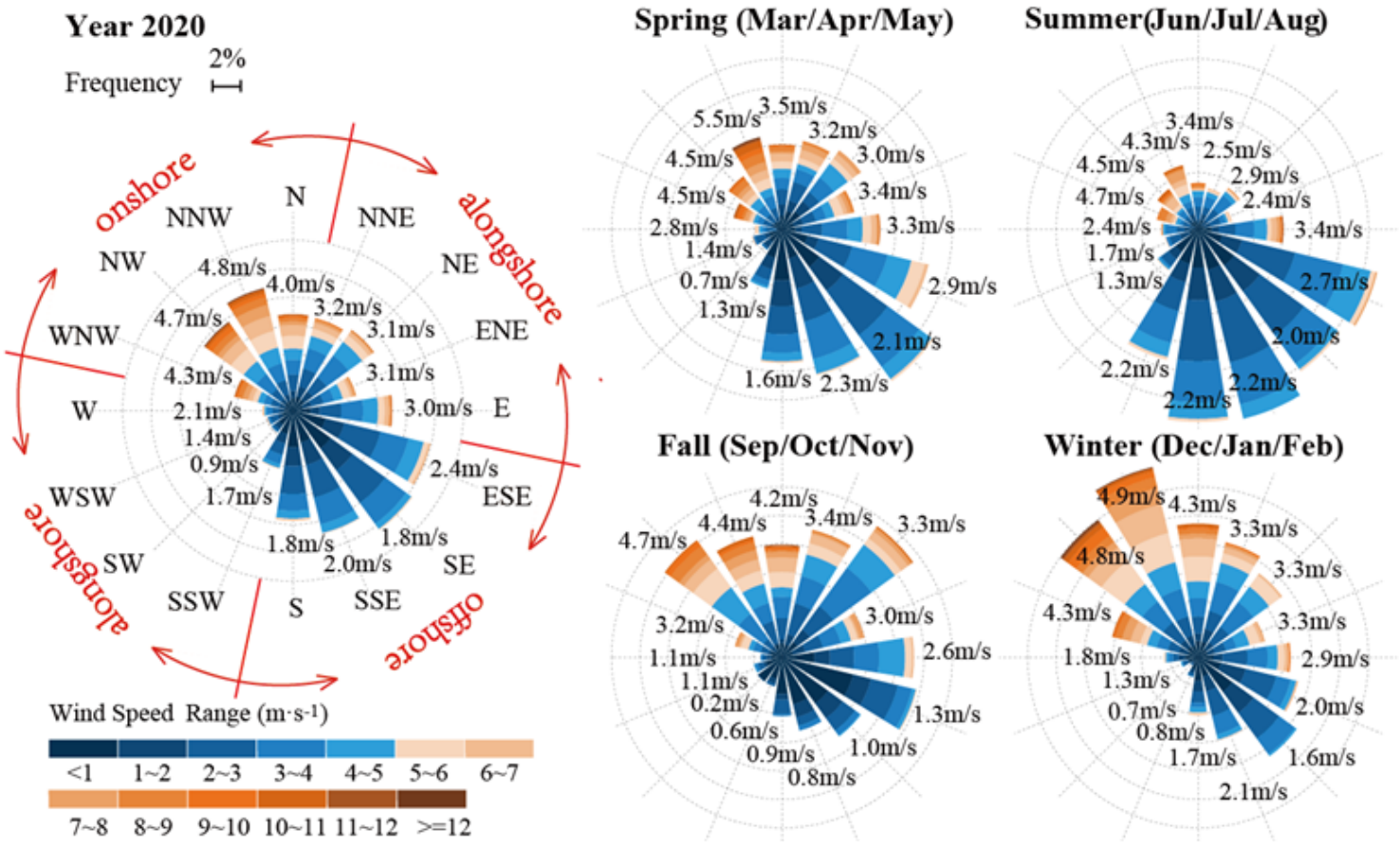

Figure 2

Wind conditions of the year 2020

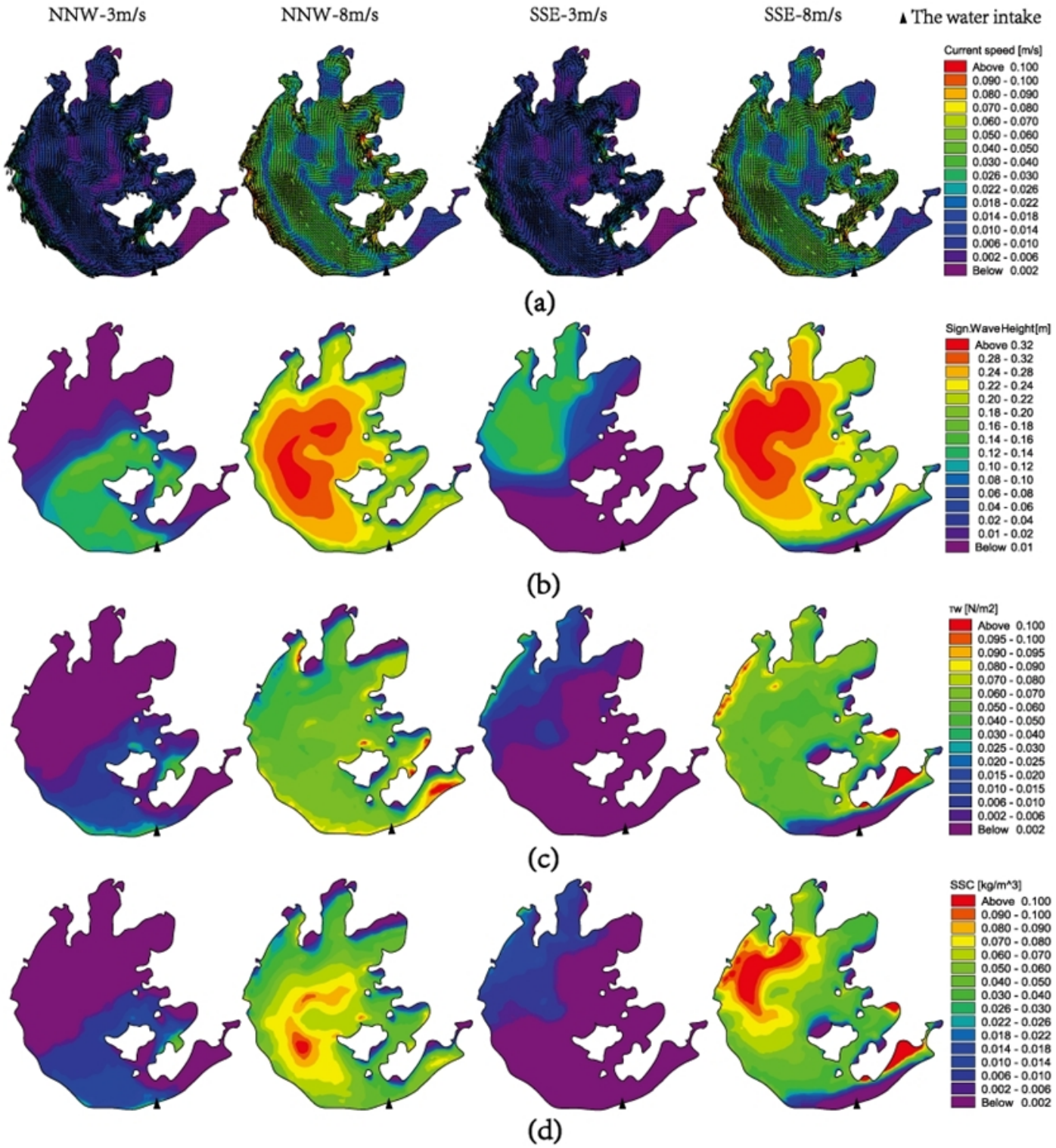

Figure 3

Field distributions at the speed of 3m/s and 8m/s under NNW and SSE winds:

(a) Current; (b) Significant wave height; (c) wave induced shear stress; (d) SSC

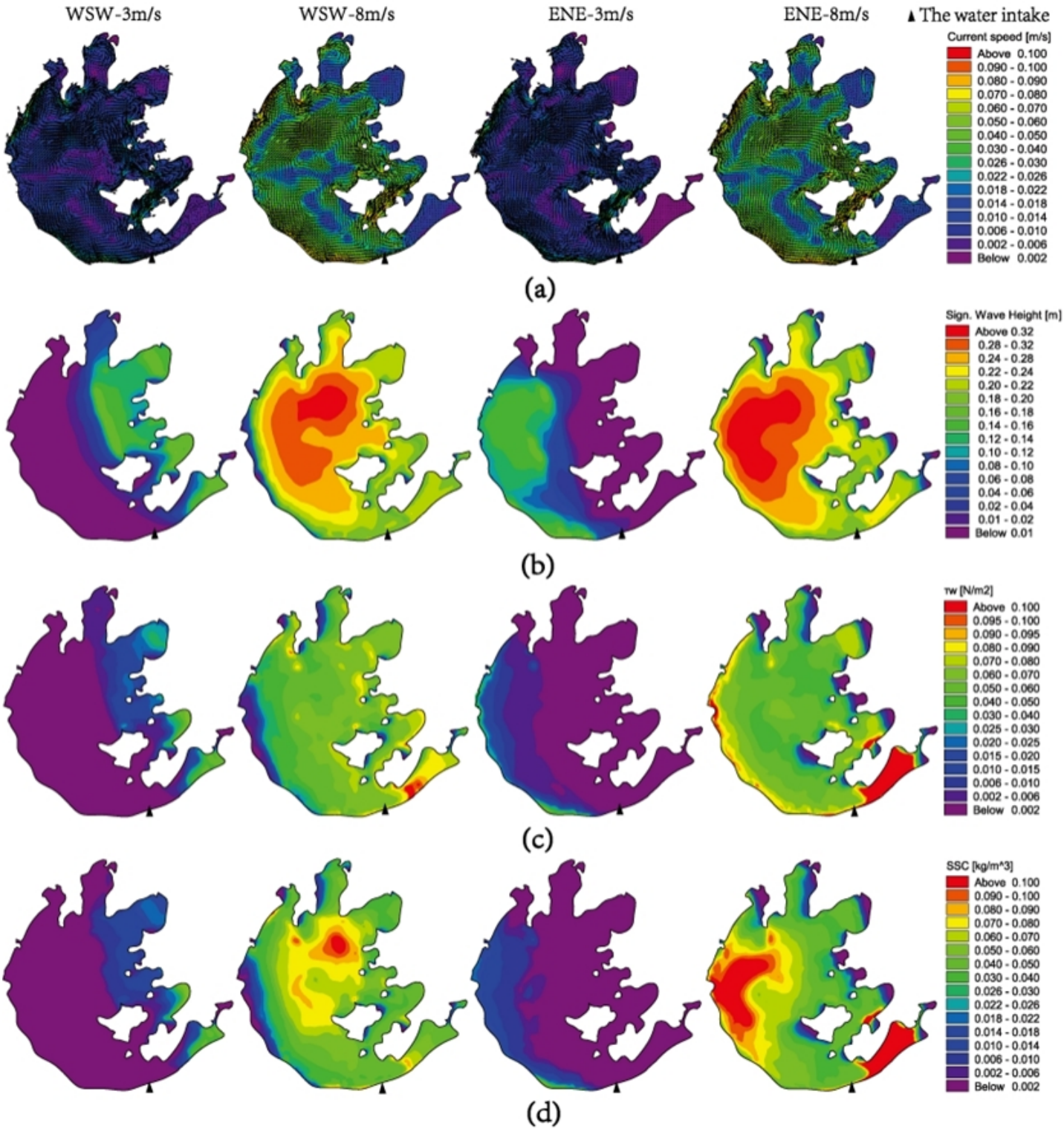

Figure 4

Field distributions at the speed of 3m/s and 8m/s under WSW and ENE winds:

(a) Current; (b) Significant wave height; (c) wave induced shear stress; (d) SSC

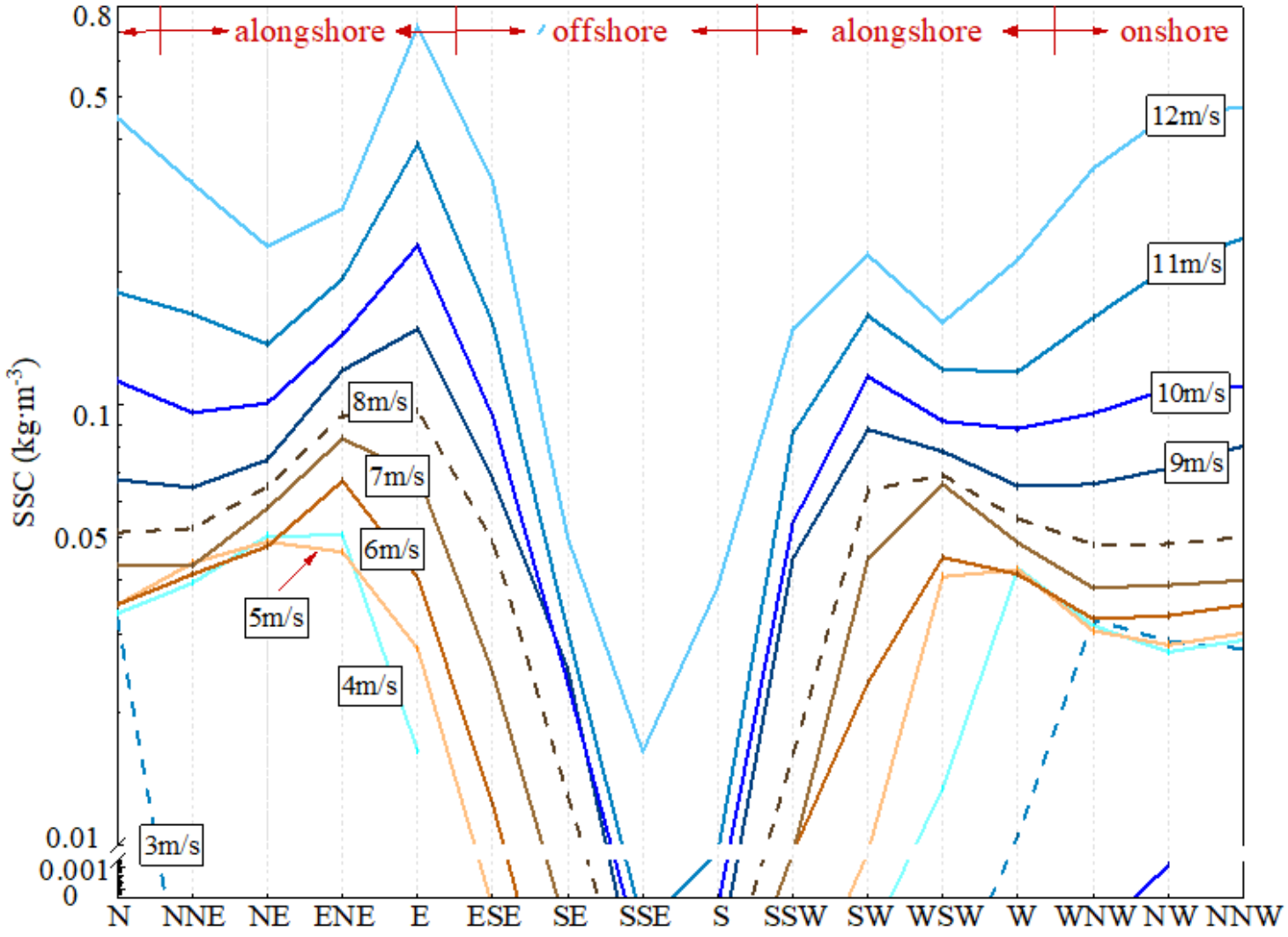

Figure 5

Simulated SSC of the water intake area under different model conditions

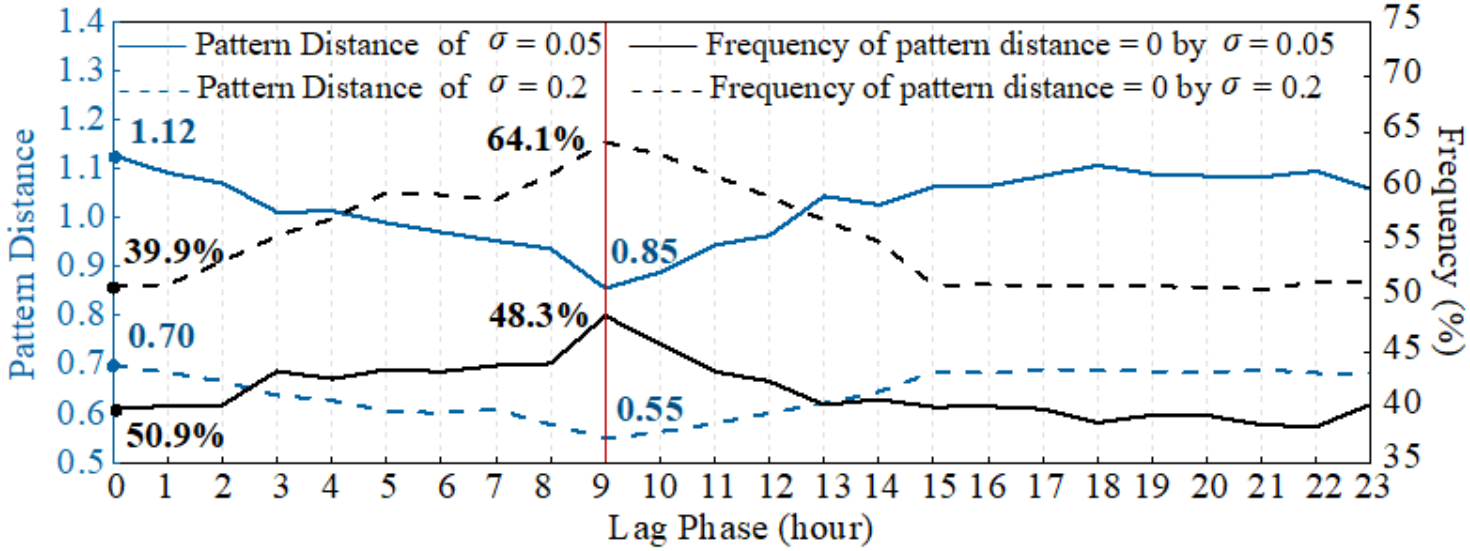

Figure 6

Thecomparison of pattern distanceunder different **σ** and lag phase

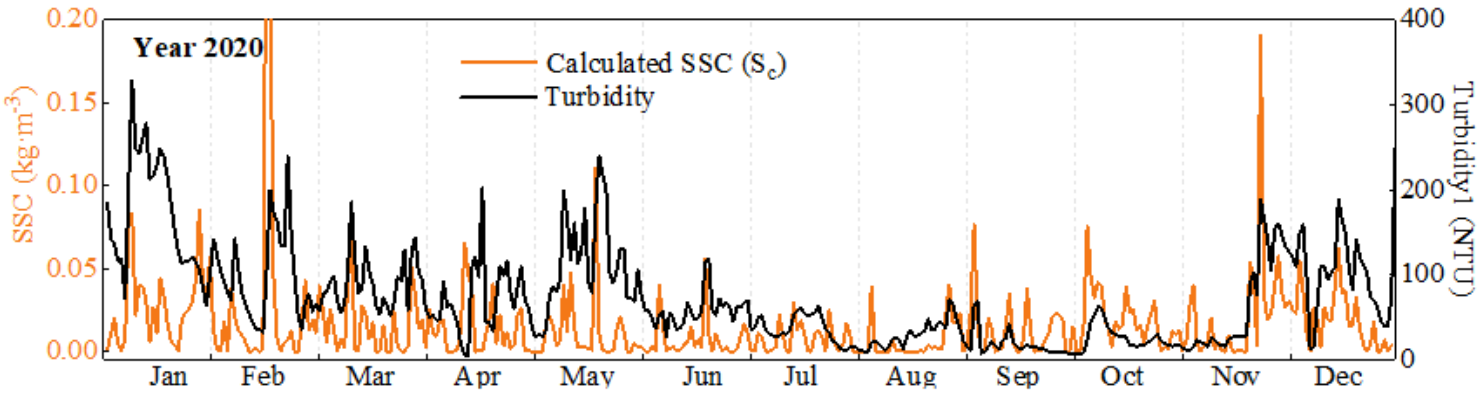

Figure 7

Day-mean series of S_C and turbidity

Supplementary Files

This is a list of supplementary files associated with this preprint. Click to download.

- ESM1.pdf.pdf